Soft Matter

Accepted Manuscript

This article can be cited before page numbers have been issued, to do this please use: I. T. Song and R. J. Stewart, *Soft Matter*, 2017, DOI: 10.1039/C7SM01654A.

ROYAL SOCIETY OF CHEMISTRY

rsc.li/soft-matter-journal

View Article Online
DOI: 10.1039/C7SM01654A

Journal Name

ARTICLE

Complex coacervation of Mg(II) phospho-polymethacrylate, a synthetic analog of sandcastle worm adhesive phosphoproteins

Received 00th January 20xx,
Accepted 00th January 20xx

DOI: 10.1039/x0xx00000x

www.rsc.org/

In Taek Song [a], Russell J. Stewart [a‡]

The highly phosphorylated Pc3 proteins, major components of the sandcastle worm adhesive, are sequestered with Mg as spherical sub-granules within heterogeneous secretory granules in adhesive gland cells. The phase behavior of a synthetic phospho-polymethacrylate analog of the Pc3 phoshoproteins, in the presense of Mg(II), was characterized to determine whether it is chemically possible for the natural adhesive components to be packaged and stored as liquid complex coacervates. Of several multivalent metal salts tested, only MgCl induced complex coacervation of the phospho-copolymer. Complex coacervates formed at Mg/P ratios from 0.5-8, and in [NaCl]s from 0-3 M. At low temperature and pH, the complex coacervates were clear and homogeneous. At higher temperatures and pH, the coacervate phases were translucent. The elastic and viscous moduli initially decreased as temperature increased, but then increased significantly near the temperature boundary between clear and translucent forms. A mechanism is proposed in which relatively weak, ionic strength-independent, outer shell crossbridging of $-PO_3^{2-}$ sidechains by $Mg[H_2O]_6^{2+}$ complex ions is responsible for the clear homogeneous lower viscosity coacervate form. At higher temperature and pH, displacement of inner shell H_2O molecules by phosphate O^- ligands creates stronger crossbridges, additional dehyration, and more viscous coacervates. The results demonstrate that Pc3 phosphoproteins can exist as condensed phospho/Mg(II) complex coacervates under conditions expected in the adhesive glands of sandcastle worms in their natural environment. Considering the common regulatory role of phosphorylation and the intracellular abundance of Mg^{2+} it is possible that soft bridging of phosphate groups by $Mg[H_2O]_n^{2+}$ may promote other regulated cellular liquid liquid phase separation phenomena.

Introduction

The role of complex coacervation, associative liquid liquid phase separation (LLPS), in creating transient phase-defined compartments within the cytoplasm has become well-recognized.[1] Complex coacervation was also proposed to play a role in the formation of condensed liquid precursors of the natural underwater adhesive of sandcastle worms [2]. Sandcastle worms, *Phragmatopoma californica,* are marine polychaetes (order Sabellaridae) that glue together composite reef-like structures in the intertidal zone of temperate coastlines worldwide using adventitiously gathered sandgrains and bits of biominerals [3, 4]. Within distinct cell types of the parathoracic adhesive gland, the sandcastle worm glue is packaged and stored in at least two types of secretory granules, referred to as homogeneous and heterogeneous, each of which contains a unique set of oppositely charged biomacromolecules [5-7]. Homogeneous secretory granules contain polycationic proteins with lysine and histidine sidechains paired with sulfated polysaccharides [6]. Heterogeneous secretory granules contain polycationic proteins, as well as a set of extremely phosphorylated serine-rich proteins, Pc3A and 3B [7]. For example, Pc3B comprises 88 mol% phosphoserine. The Pc3 phosphoproteins are complexed with Mg(II) ions at a molar ratio of approximately 0.5 Mg(II) for each Pc3 phosphate sidechain in polydisperse spherical sub-granules within the heterogeneous secretory granules [5, 8]. Both types of adhesive precursor granules are transported intact and unmixed to the surface of the building organ through long cellular extensions. Soon after secretion, the modular adhesive precursors fuse into a loading-bearing microporous solid foam [7,9].

A condensed phase-separated liquid complex coacervate is in theory an ideal morphology for packaging, storing, and delivering concentrated adhesive proteins to surfaces submerged in seawater. The phase-separated liquid does not quickly disperse or dissolve when secreted into seawater, adheres to and spreads on wet interfaces, and penetrates gaps between particles by capillarity [7]. Changes in solution conditions upon secretion trigger phase inversion into a porous solid. However, direct microscopic demonstration of a liquid

[a] Department of Bioengineering, University of Utah, 20 S. 2030 East, Salt Lake City, UT 84112, USA.

Electronic Supplementary Information (ESI) available: [details of any supplementary information available should be included here]. See DOI: 10.1039/x0xx00000x

View Article Online
DOI: 10.1039/C7SM01654A

morphology of the sandcastle worm adhesive within the intact adhesive gland cells is experimentally challenging. As an alternative approach, we characterized the Mg(II) ion induced complex coacervation of a phosphomethacrylate synthetic analog of the Pc3B protein, (poly)phosphoethyl methacrylate-co-hydroxyethyl methacrylate (p(PEMA-co-HEMA)). The synthetic copolymer mimics the phosphoester-terminated sidechains, the high mol% of phosphate sidechains, the M_m, and unstructured nature of Pc3B. The synthetic Pc3 analog separated into clear homogeneous liquid phases in the presence of Mg(II) within a narrow range of temperature and pH, and into translucent inhomogeneous liquid phases at higher temperatures and pH.

Materials and methods

Materials

Phosphorus(V) oxychloride and 2-hydroxyethyl methacrylate (HEMA) were purchased from Alfa Aesar (Ward Hill, MA). Triethyl amine (TEA), azo-bis-isobutyronitrile (AIBN), Magnesium chloride hexahydrate ($MgCl_2$ $6H_2O$) were purchased from Sigma Aldrich (St Louis, MO). Toluene (Fisher Scientific) was dried over 4 angstrom molecular sieves (Mallinckrodt Chemicals).

Phosphate monomer synthesis

2-(phosphonooxy)ethyl methacrylate (PEMA) was synthesized as described previously [11]. Briefly, phosphorus(V) oxychloride (33.9 g, 220 mmol) was mixed with HEMA at a 0.7 to 1.0 molar ratio in dry toluene (480 ml) under argon. The reaction was stirred at 4° C while triethylamine (TEA) (78 ml) was added slowly over 10 min. Following addition of TEA, the reaction was stirred under argon for 6 h at 21-23° C, then filtered to remove precipitated TEA-HCl salt. The reaction was cooled to 4° C before addition of DI water (480 ml), then stirred under argon at 21-23° C for 12-15 hr. The reaction was extracted twice with diethyl ether (100 ml) to remove unreacted HEMA. The product, PEMA, was then extracted with tetrahydrofuran (THF) and diethyl ether (1:2, 8 x 200 ml). The monomer structure was verified by ^1H and ^{31}P NMR using a Varian Mercury 400. Yellow oil; ^1H NMR (D_2O, 400 MHz); 6.05 (s, 1H), 5.68 (s, 1H), 4.23 (t, J = 4 Hz, 2H), 4.02 (t, J = 4 Hz, 2H), 1.87 (s, 3H). ^{31}P NMR (D_2O, 400 MHz), -1.206 (s).

Synthesis and characterization of p(PEMA-co-HEMA)

p(PEMA80-co-HEMA20) was synthesized by free radical polymerization of 24 g of PEMA and 3.7 g of HEMA in methanol (13.9 ml/1g of PEMA) at a molar feed ratio of 80:20 PEMA to HEMA as previously described (scheme 1) [11]. The reaction was initiated with AIBN, 4.5 mol% at 55 ° C, and stirred 12-15 hr. The product was precipitated with 2 L of acetone, then dissolved in water (200 ml H_2O per 17 g PEMA). The p(PEMA-co-HEMA) was purified by washing with 10 volumes of water on a tangential flow filtration system using a Millipore Pellicon 3 cassette filter with an Ultracel 10 kD membrane. The pH of the p(PEMA-co-HEMA) solution was adjusted to 7.3 with NaOH, then lyophilized, and stored as the sodium salt at -20° C.

The final polymer comprised 65.0 and 35.0 mol% phosphoethyl and hydroxyethyl sidechains, respectively, as determined by ^1H and ^{31}P NMR spectroscopy. The M_m and polydispersity index (PDI) of p(PEMA65-co-HEMA35) were 56 kg/mol and 1.6, respectively, as determined by size exclusion chromatography (SEC) using an Agilent PL-Aquagel-OH MIXED-M, 8µm, 300 x 7.5 mm column on an Agilent 1250 system (Agilent Technologies) equipped with refractive index (RI) and light scattering (Wyatt MiniDawn Treos) detectors. Copolymer samples were prepared and run in 0.1M $NaNO_3$/0.01M NaH_2PO_4 (pH 8.0) at 1 ml/min. For comparison to the natural phosphoprotein, the M_m of fully phosphorylated Pc3B is ~57 kg/mol.

Mg(II) induced p(PEMA-co-HEMA) coacervation

p(PEMA65-co-HEMA35) was dissolved at 50 mg/mL in water. For determining the ionic strength dependence of coacervation NaCl was added to the copolymer solution in concentrations ranging from 0 to 3.0 M before coacervation was induced by addition of $MgCl_2$. To investigate the pH dependence, the pH of the copolymer solution was adjusted over the range 4.0 to 12.5 with NaOH before addition of $MgCl_2$. Coacervation was induced by the addition of unbuffered aqueous solutions of 2.67 M $MgCl_2$ to give final concentrations ranging from 50 to 1600 mM corresponding to molar ratios of Mg(II) to phosphate ranging from 0.25 to 8. The coacervated solutions were equilibrated for a minimum of 16 hrs. All steps were done at 20-22° C.

Characterization and analysis of Mg(II) induced p(PEMA65-co-HEMA35) coacervate

The mass of p(PEMA65-co-HEMA35) in the coacervate phase was determined by precipitating copolymer in the equilibrium phase (supernatant) with $CaCl_2$. 50 mg of $CaCl_2$ was added to 100 µl of supernatant solution, which was then centrifuged for 10 min at 6,000 rpm. After removing the supernatant, the precipitate was washed 5X with distilled water, then dried in a vacuum oven. The mass of polyphosphate in the precipitate was calculated by subtracting the weight of Ca^{2+}, assuming the precipitate was predominantly in the form $-ROPO_3^{2-}$ Ca^{2+}. The mass of p(PEMA65-co-HEMA35) in the coacervate was determined by subtracting the supernatant copolymer mass from the total copolymer mass added to the solution.

View Article Online
DOI: 10.1039/C7SM01654A

A phase diagram was constructed by preparing p(PEMA65-co-HEMA35) solutions (200 mg/ml) at a fixed Mg/P ratio of 4. The pH was adjusted to range from 4 to 12 and the temperature of each sample was varied from 4 to 60°C in a thermal cycler (PTC-150 PCR Mini cycler, MJ Research). After equilibrating, the morphology of the solution was visually determined as no phase separation, clear homogeneous complex coacervates, and translucent viscous complex coacervates. For some complex coacervates the elastic (G') and viscous (G'') moduli as a function of temperature and [NaCl] by oscillatory rheology (AR2000ex, TA Instruments), using a 20 mm 4° cone at 1 hz and 1% strain. A solvent trap was used to prevent sample dehydration.

Dianionic and monoanionic vibrational modes of the phosphate groups were used to titrate respective functional groups using ATR-FTIR. Coacervates (pH 5, 5.5, 6, 6.8, 7.7, 8, 8.1 and 8.5) and solution samples (pH 3.2 and 4.1) were lyophilized for FTIR analysis. The wavenumbers of phosphate group were specifically monitored from 1400 cm^{-1} to 800 cm^{-1}. Major water absorbance, 3500 cm^{-1}, 2120 cm^{-1}, did not overlap with the phosphate region of the spectra. ATR-FTIR absorbance spectra were collected using a Nicolet 6700 spectrometer (Thermo Scientific, FL) with a diamond Smart iTR accessory, a deuterated triglycine sulfate detector, and a KBr/Ge mid-infrared optimized beam splitter. All spectra were recorded with a resolution of 4 cm^{-1} and 512 averaged scans. The spectra were normalized using the 1707 cm^{-1} band from the C=O stretching mode. The peaks were fit and integrated using the 2nd derivatives mode in PeakFit curve fitting software (Seasolve Software Inc.)

Results

Complex coacervation of Mg^{2+}/p(PEMA65-co-HEMA35)

Addition of Mg^{2+} ions, at a 2:1 ratio of Mg^{2+} to phosphate sidechains, to a solution (pH 6.0) of the sodium salt of p(PEMA65-co-HEMA35) resulted in immediate and quantitative aggregation of the copolymer into a white gelatinous mass that settled under gravity to the bottom of the tube. After 18 hr at 20-22°C, the initial aggregation transitioned into a clear homogenous liquid phase (Fig. 1). To determine if other metal ions would induce similar LLPS, a series of multivalent metal ions (Al^{3+}, Zn^{2+}, Ba^{+}, Ca^{2+}, Mn^{2+}, Cr^{3+}, Fe^{3+}, Cu^{2+}, Ni^{2+}) were added to solutions (pH 6.8) of sodium p(PEMA65-co-HEMA35) at a 2:1 ratio of metal ion to phosphate sidechains at 20-22 °C. As expected, most of the multivalent metal ions generated solid flocs. Ni^{2+} formed dense green gels. Mg^{2+} was the only metal ion tested that formed

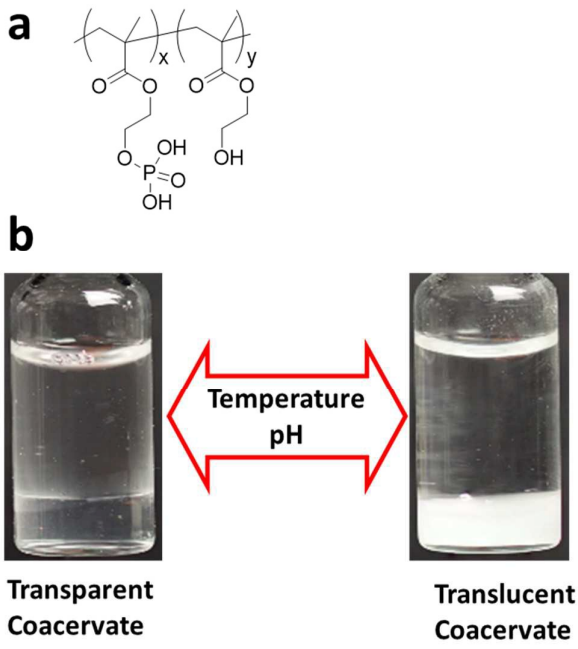

Fig. 1 Mg^{2+}/PEMA complex coacervation. A.) Structure of pPEMA-co-HEMA. B.) Transparent complex coacervates formed at low temperature and pH. Translucent complex coacervates formed at higher temperatures and pHs. The forms were interconvertible by changing the solution conditions.

liquid complex coacervates with p(PEMA65-co-HEMA35) within the pH and temperature range explored.

The phase behavior of the organic pPEMA copolymers is distinct from inorganic polyphosphates ($[NaPO_3]_n[NaPO_3(OH)]_2$), which have been reported to form phase separated complex coacervates with several multivalent metal ions, including Mn^{2+}, Ni^{2+}, Fe^{3+}, Ca^{2+}, Zn^{2+}, Al^{3+}, and Mg^{2+}.[12-23] Inorganic polyphosphates are connected through phosphodiester bonds. Therefore only one phosphorus oxygen per unit is available to participate in metal ion complexes, whereas the phosphate sidechains of the pPEMA copolymer have two phosphorus oxygens available for metal coordination, as do the phosphate sidechains of phosphoproteins such as the sandcastle worm Pc3s. The intermolecular metallo-phosphate crosslinks of inorganic polyphosphates may be weaker and more dynamic than the metallophosphate complexes of dianionic pPEMA, which forms solid precipitates with most metal ions, and a liquid morphology only with Mg^{2+} ions.

View Article Online
DOI: 10.1039/C7SM01654A

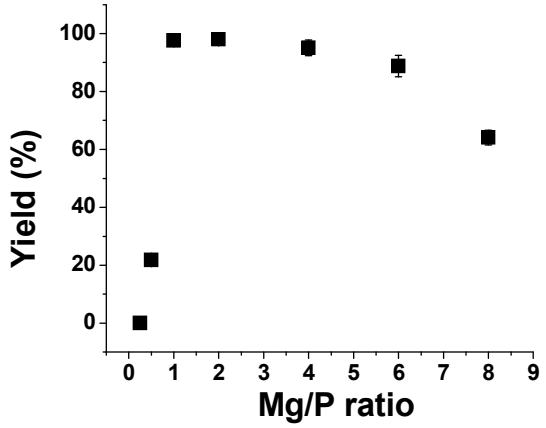

Fig. 2 Coacervate yield vs. Mg/P ratio. Yield is the percent of total copolymer in the complex coacervate phase.

To further investigate Mg^{2+} induced coacervation of p(PEMA65-co-HEMA35), the dependence on Mg^{2+} ion to phosphate sidechain stoichiometry was determined at Mg/P ratios ranging from 0.25 to 8. Before adding Mg^{2+} the copolymer solutions were adjusted to pH 9.0 in 100 mM borate buffer so that the phosphate sidechanis were dianionic. A coacervate phase did not form at Mg/P ratios of 0.25. At a Mg/P ratio of 0.5, 22 % of the copolymer phase separated into a complex coacervate. At ratios between 1 and 4, greater than 95% of the copolymer was in the coacervate phase. At ratios of 6 and 8, the yield decreased to 88 and 64 %, respectively (Fig. 2). Coacervation occurred efficiently at super-stoichiometric Mg/P ratios, and therefore, super-stoichiometric positive to negative charge ratios, in contrast to the nearly 1:1 charge ratio typically observed in complex coacervates mediated through non-specific electrostatic interactions [24-26].

Ionic strength dependence of Mg^{2+}/p(PEMA65-co-HEMA35) complex coacervation.

Complex coacervation mediated through non-specific electrostatic interactions between oppositely charged polyelectrolytes is sensitive to ionic strength. The higher the concentration of counter ions the greater the shielding of interactions between polymeric ions [25-29]. Thus, increasing salt concentration decreases the amount, density, and viscosity of the complex coacervate phase. At sufficiently high salt concentration no coacervate phase is formed [29, 30]. In contrast, Mg^{2+} induced complex coacervation of p(PEMA65-co-HEMA35) was independent of the NaCl concentration. At a Mg/P ratio of 4, at pH 9 and at 22 °C, >95 % of the copolymer was in the coacervate phase at NaCl concentrations ranging from 0 mM to 3000 mM (Fig. 3a). Under these conditions, all of the complex coacervates were translucent (Fig. 1b) likely due to micro-phase separation of water within the coacervate macrophase.

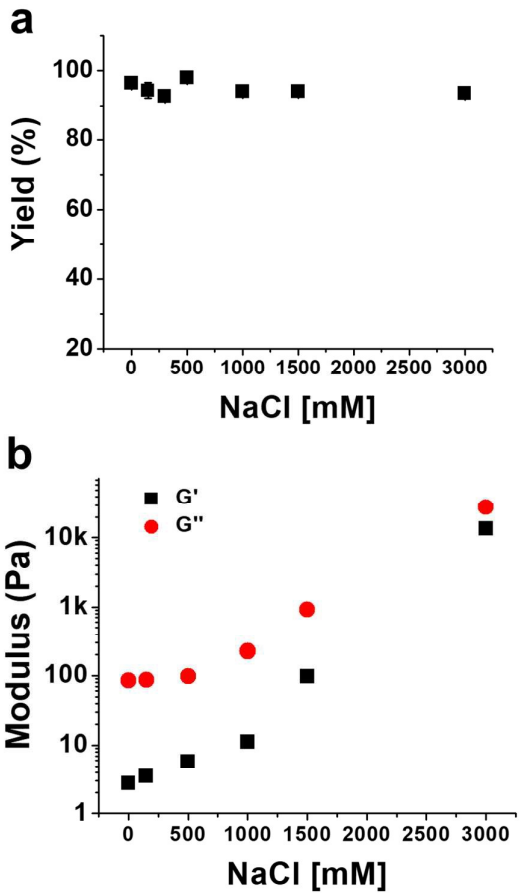

Fig. 3 Ionic strength dependence of Mg^{2+}/pPEMA-co-HEMA complex coacervation. a) Coacervate yield vs. NaCl concentration. Yield is defined as the amount of total copolymer in the coacervate phase. b) Elastic modulus (G', black) and viscous modulus (G'', red) vs. NaCl concentration. For all coacervates: Mg/P ratio = 4, pH = 6.3, 20-22 °C

In further contrast to electrostatic complex coacervates,[29,30] higher NaCl concentrations increased both the elastic (G', black symbols) and viscous (G", red symbols) moduli of the Mg^{2+}/p(PEMA65-co-HEMA35) complex coacervates, as measured by oscillatory rheology (Fig. 3b). The G' at 0 mM NaCl was 3 Pa vs. 10,000 Pa at 3 M NaCl at 1 Hz and 1% strain. The mechanism underlying the increasing stiffness with increasing [NaCl] requires further study. It may be due to osmotic dehydration of the complex coacervate phase by a higher [NaCl] in the equilibrium phase, which would remove plasticizing water. At all NaCl concentrations tested, the viscous modulus was greater than the elastic modulus, indicating that the complex coacervates were viscous fluids rather than elastic gels. At a fixed temperature, the elastic modulus also increased with pH although less dramatically. At pH 5.0, 8.0, and 8.5 the G' was 36, 132, and 994 Pa, respectively.

View Article Online
DOI: 10.1039/C7SM01654A

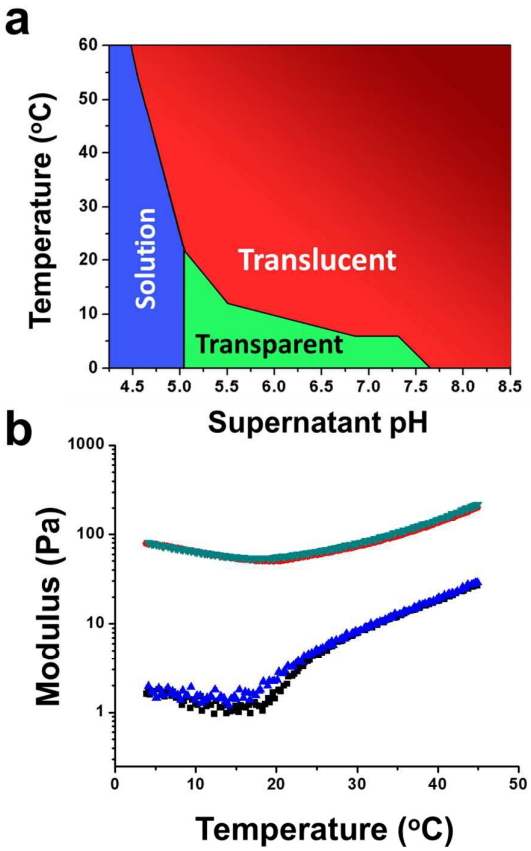

Fig. 4 a) Phase and morphology diagram of Mg^{2+}/pPEMA-co-HEMA vs. temperature and pH. Blue area = solution, green = transparent coacervates, red area = translucent coacervate. b) Rheology temperature sweep of pH 6.3 coacervate. G' values from 4 to 45 °C (black) and from 45 to 4 °C (blue). G'' values from 4 to 45 °C (red) and from 45 to 4 °C (green) (Mg/P = 4:1).

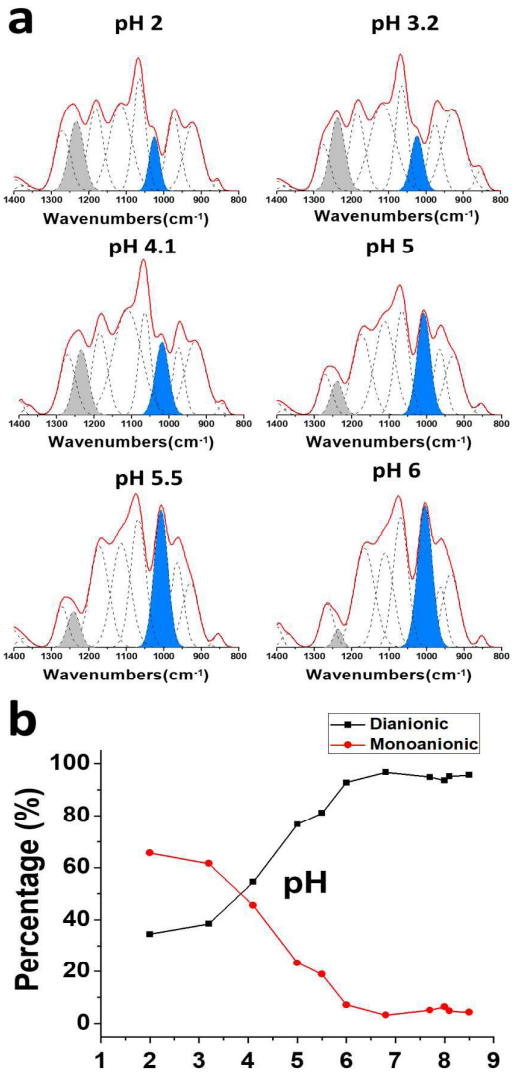

Fig. 5 Phosphate ionization determined by ATR-FTIR. a) FTIR spectrums at different pH. Gray peak represents monoanionic phosphate. Blue peak represents dianionic phosphate. b) Percentage of dianionic (black) and monoanionic (red) groups from a).

Mg^{2+}/ p(PEMA65-co-HEMA35) phase diagram

Based on the above results, the Mg/P ratio was fixed at 4 and the NaCl concentration at 150 mM to create a map of the morphology of the resulting solutions as a function of pH and temperature (Fig 4a). Below pH 5, complex coacervate phases did not form except at elevated temperatures (blue region). In a narrow range between pH 5-7.5 and less than 20 °C, the complex coacervate was in the transparent form (green region). Outside of these regions the complex coacervate was translucent (red region). The wt% water in the transparent and translucent forms in 150 mM NaCl were similar, 58.9 ± 0.9 and 57.1 ± 2.4, respectively.

Temperature dependent transitions between the transparent and translucent forms of the complex coacervate were reversible. This was apparent visually and also demonstrated by the temperature dependence of the elastic and viscous moduli (Fig. 4b). With the pH fixed at 6.3, the temperature was ramped from 4 to 45 °C. The moduli decreased slightly as the temperature was raised until it reached the approximate boundary between the transparent and translucent forms, at which point the moduli increased substantially with temperature. The moduli decreased along the same path when the temperature ramp was reversed. The initial decrease, then abrupt increase in moduli suggested a reorganization in the solution structure during the transition from the transparent to translucent forms.

Phosphate sidechain ionization

The ionization state of the phosphates sidechains was determined by ATR-FTIR of Mg^{2+}/p(PEMA65-co-HEMA35) solutions and coacervates prepared over a range of pH values

View Article Online
DOI: 10.1039/C7SM01654A

with the Mg/P ratio fixed at 4:1 (Fig. 5a). The peak centered at 1238 cm^{-1}, corresponds to the monoanionic phosphate asymmetric stretching mode [31, 32]. The peak centered at 1002 cm^{-1} corresponds to the dianionic phosphate symmetrical stretching mode [31, 32]. The integrated values of the peaks were plotted against pH (Fig. 5b). The mid-point of the transition from monoanionic to dianionic, an estimate of $pK_{a2,}$ was near pH 4. In the presence of Mg^{2+}, the pK_{a2} of the PEMA phosphate sidechains was shifted substantially lower than the pK_{a2} (~7.2) of $H_xPO_4^{-n}$. Similar shifts in pK_{a2} have been observed in monolayers of phosphatidic acid in the presence of multivalent metal ions[33] and H-bonds [34] that promote deprotonation of the phosphate groups at low pH. Complex coacervation of Mg^{2+}/p(PEMA65-co-HEMA35) only occurred at and above pH 5 (Fig. 4a) when approximately 80% of the phosphate sidechains were dianionic. At pH 5, 80% of the copolymer was in the clear homogeneous coacervate phase, which suggested that predominantly dianionic phosphate sidechains participated in associative phase separation with Mg^{2+}.

Discussion

Mechanism of complex coacervation. Of the several metal ions compared, why does Mg^{2+} uniquely lead to the condensation of pPEMA-co-HEMA into a liquid complex coacervate rather than a solid precipitate? The answer likely lies in the rigid hydration shell of aquated Mg^{2+}. In water, Mg^{2+} has six H_2O molecules in an inner coordination shell, oxygen atoms directed inward, packed into a tight octahedral geometry [35-38]. An additional 12 water molecules are hydrogen-bonded in an outer coordination shell (Fig. 6) [36]. Evidence for the high stability of the $Mg[H_2O]_6^{2+}$ complex ion compared to other multivalent metal complex ions comes from numerous theoretical studies [35, 36, 38, 39], and empirically from investigation of Mg^{2+} containing crystal structures of small organic compounds [35] and proteins [38, 40]. In these structures, it is common to find coordinated Mg^{2+} ions that have retained all six inner sphere water molecules in the presence of oxygen ligands of carboxylates and phosphates.

In effect, the +2 charge of the central Mg^{2+} ion is distributed into the partial positive charges of the hydrogen atoms of the inner shell water molecules. Taking the constrained inner hydration shell into account, the volume of the $Mg[H_2O]_6^{2+}$ complex ion is 400 times greater than the volume of the Mg^{2+} ion [41]. Although Mg^{2+} is a small ion with high charge density, the stable $Mg[H_2O]_6^{2+}$ complex is a large ion with low surface charge density. The stability and low surface charge density of $Mg[H_2O]_6^{2+}$ together explain its relatively weak crosslinking of pPEMA-co-HEMA phosphate sidechains. The crosslinks are sufficiently energetic to cause associative phase separation of the polyelectrolyte, but weak and sufficiently dynamic to create a liquid rather than a solid morphology. For comparison, aquated Ca^{2+} ions, which create solid precipitates of pPEMA-co-HEMA, have a flexible coordination number of 6-9 [42]. The volume of hydrated Ca^{2+} is <1/4 the volume of hydrated Mg^{2+} [41].

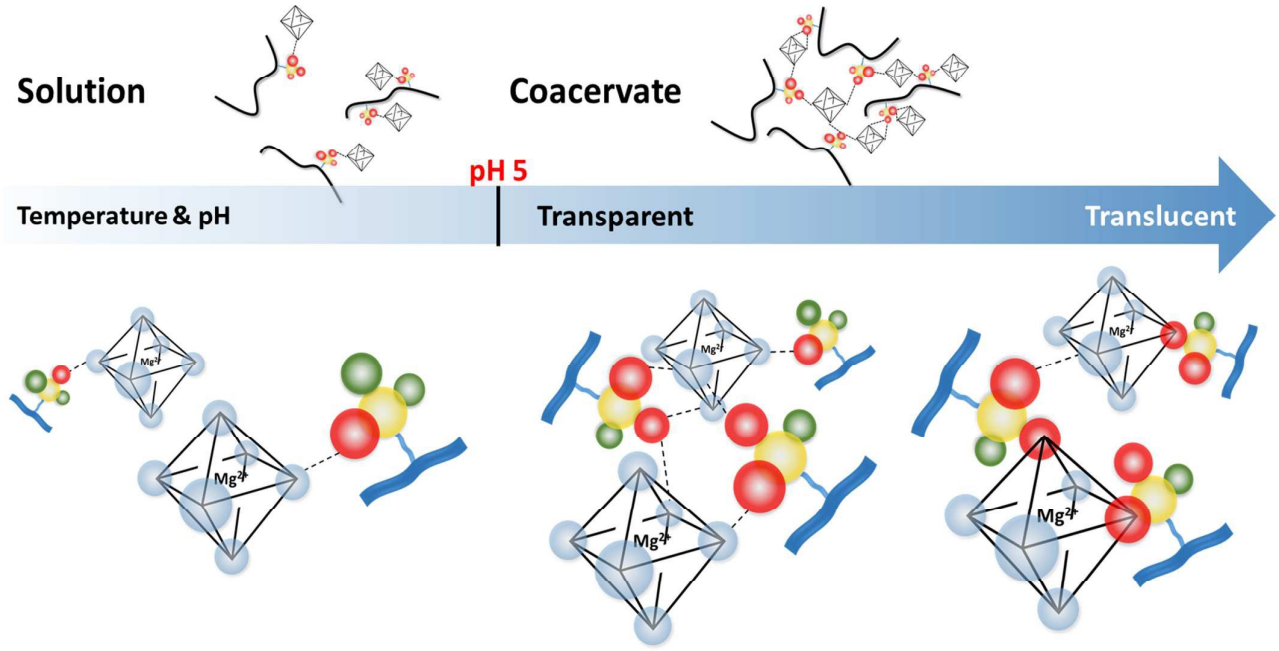

Fig.6 Mechanism of coacervation. Gray spheres = Mg^{2+} inner shell water molecules. Yellow spheres = phosphorus. Green spheres = protonated phosphate oxygens. Red spheres = deprotonated phosphate oxygens. Complex coacervation does not occur at low temperature and pH. Complex coacervation begins at the pH where the phosphates are double ionized and is mediated through outer shell H-bonds (dashed lines) resulting in the transparent form. At higher temperature and pH, exchange of inner shell H_2O molecules by $P\text{-}O^-$ creates stronger inner shell Mg-O coordination bonds that increase the viscosity of the coacervate. The translucence at higher T and pH is likely due to additional dehydration and formation of light scattering water microphases.

View Article Online
DOI: 10.1039/C7SM01654A

The exchange rate of inner shell H_2O molecules is 3-4 orders of magnitude faster for Ca^{2+} than Mg^{2+} [43]. As a result, Ca^{2+} is more readily dehydrated to form strong inner sphere coordination complexes with phosphate O^- ligands, resulting in solid precipitates of pPEMA-co-HEMA rather than a liquid coacervate.

In this context, we note similar behavior in a natural structural material—the underwater silk of caddisworms. The strength, toughness, and energy-dissipating strain cycle hysteresis of caddisworm silk are due to serial β-domains stabilized by exchangeable Ca^{2+}/phosphoserine complexes in repeating (pSX_4) phosphoserine (pS) motifs of H-fibroin [32, 44-46]. Exchange of native Ca^{2+} with Na^+ results in swelling of the silk fibers, changes in pSX_4 β-domain structure, and the complete disruption of their strength and energy-dissipating hysteresis. When Ca^{2+} is exchanged with Mg^{2+}, in contrast to Na^+, the fibers do not swell, and although the pSX_4 β-domains remain intact as evident from ATR-FTIR spectroscopy, Mg^{2+} ions impart very little strength or hysteresis to the fibers [47]. Compared to Ca^{2+}/pSX_4 complexes, the Mg^{2+}/pSX_4 complexes offer little resistance to fiber stretching and β-domain unfolding. Similar metal ion comparative effects on mechanical behavior were reported in metallophosphate double network hydrogels [11].

The extent of $Mg^{2+}[H_20]_6^{2+}$-induced coacervation of pPEMA-co-HEMA was not affected by NaCl concentrations as high as 3 M. In fact, the viscosity increased significantly at higher [NaCl] in contrast to complex coacervation mediated through non-specific electrostatic interactions [30, 48]. This is an important property for adhesives, such as the sandcastle worm glue, that are applied and harden in seawater, in which the concentration of NaCl is ~ 500 mM. The insensitivity to [NaCl] demonstrates that the weak intermolecular bonding mechanisms responsible for the cohesion of the $Mg[H_20]_6^{2+}$/pPEMA-co-HEMA complex coacervates are not non-specific electrostatic interactions.

As diagrammed in figure 6, we propose complex coacervation of pPEMA-co-HEM is primarily driven through H-bonds and specific coordinate bonds rather than electrostatic bonds. At pH < 5 with mostly monoanionic sidechains the polyphosphate is not coacervated by $Mg[H_20]_6^{2+}$ and remained fully solvated. At pH ≥ 5 and low temperatures—the clear homogeneous region of the phase diagram—bonding is primarily through NaCl insensitive H-bonds between fully hydrated $Mg[H_20]_6^{2+}$ ions and dianionic $–O\text{-}P\text{-}O_3^{2-}$ sidechains. At higher temperatures and pH—the inhomogeneous translucent region of the phase map—increased cohesion is due to partial displacement of inner shell H_2O molecules with phosphate oxygen anions to form NaCl insensitive coordinate bonds. The transition from primarily H-bonds to coordinate bonds strengthens the metalophosphate complexes, increasing the viscosity and cohesiveness of the liquid complex coacervate phase. Additional dehydration may release water that becomes sequestered in light scattering microphases causing the complex coacervate to become translucent.

Mg^{2+} is a hard acid that preferentially interacts with hard bases, like the oxygen anions in carboxylates and phosphates. In general, complexes between hard bases and hard acids are predominantly electrostatic, with little covalency or charge transfer [49]. However, evidence that Mg^{2+}/phosphate complexes are at least partially coordinative comes from the failure of simple electrostatic models to explain $Mg[H_20]_6^{2+}$ coordination by RNA [50, 51]. $Mg[H_20]_n^{2+}$ ions play a critical role in the folding of structured RNA molecules. The $Mg[H_20]_n^{2+}$ ions are bound through two modes: diffuse binding and site binding. Diffuse Mg^{2+} ions remain fully hydrated, whereas site bound Mg^{2+} frequently have one or two H_2O molecules displaced by inner shell $P\text{-}O^-$ ligands [52, 53]. Although, electrostatic models account for diffuse binding through outer shell coordination, there are non-electrostatic contributions to site bound $Mg[H_2O]_n^{2+}$ complexes in which phosphate O^- ligands have displaced inner sphere H_2O molecules.

Conclusions

Phragmatopoma californica sandcastle worms live in a marine environment where the water temperature annual range is between 14-18 °C [54]. The adhesive granule pH and ionic strength has not been directly measured. However, it is reasonable to expect the pH to be greater than 5 and the contribution of inorganic monovalent ions to the internal ionic strength to be similar to other eukaryotes[55]. These natural conditions lie in the low viscosity, clear complex coacervate region of the pPEMA-co-HEMA/ $Mg[H_2O]_n^{2+}$ phase diagram (Fig. 4B), which suggests it is chemically and physically possible the Pc3 proteins are sequestered in the heterogeneous sub-granules in the form of concentrated liquid complex coacervates by weak complexation with $Mg[H_2O]_n^{2+}$ complex ions. Upon secretion into seawater at pH 8.2, exchange of $Mg[H_2O]_n^{2+}$ with Ca^{2+}, with its greater tendency to form inner sphere complexes, would further dehydrate and harden the Pc3 metallo-complexes in the adhesive joint. Liberated water may coalesce into microphases to form the microporous foam structure of the final adhesive bond [2, 9].

Finally, considering the regulatory role of phosphorylation and the intracellular abundance of Mg^{2+} it is possible that intermolecular soft bridging of phosphate groups by $Mg[H_2O]_n^{2+}$ may promote other regulated, or pathological, cellular LLPS phenomena.

Conflicts of interest

There are no conflicts of interest to declare.

Acknowledgements

Grants from the Office of Naval Research #N00014-16-1-2538, the National Institutes of Health #HD75863, and the Army Research Office #W911NF1310319 are gratefully acknowledged.

View Article Online
DOI: 10.1039/C7SM01654A

Notes and references

‡ Corresponding author

1. A. A. Hyman, C. A. Weber and F. Juelicher, *Annu Rev Cell Dev Bi*, 2014, **30**, 39-58.
2. R. J. Stewart, J. C. Weaver, D. E. Morse and J. H. Waite, *J Exp Biol*, 2004, **207**, 4727-4734.
3. J. Vovelle, *Archives de zoologie expérimentale et générale.*, 1965, **106**, 187.
4. S. Dubois, L. Barille, B. Cognie and P. G. Beninger, *Mar Ecol Prog Ser*, 2005, **301**, 159-171.
5. C. S. Wang and R. J. Stewart, *J Exp Biol*, 2012, **215**, 351-361.
6. C. S. Wang and R. J. Stewart, *Biomacromolecules*, 2013, **14**, 1607-1617.
7. R. J. Stewart, C. S. Wang, I. T. Song and J. P. Jones, *Adv Colloid Interface Sci*, 2017, **239**, 88-96.
8. C. P. Brangwynne, *J Cell Biol*, 2013, **203**, 875-881.
9. M. J. Stevens, R. E. Steren, V. Hlady and R. J. Stewart, *Langmuir*, 2007, **23**, 5045-5049.
10. C. P. Brangwynne, C. R. Eckmann, D. S. Courson, A. Rybarska, C. Hoege, J. Gharakhani, F. Julicher and A. A. Hyman, *Science*, 2009, **324**, 1729-1732.
11. D. D. Lane, S. Kaur, G. M. Weerasakare and R. J. Stewart, *Soft Matter*, 2015, **11**, 6981-6990.
12. L. F. C. de Oliveira, M. A. P. Silva, A. R. Brandao, R. Stephani, C. I. R. de Oliveira, R. R. Goncalves, A. J. Barbosa, H. S. Barud, Y. Messaddeq and S. J. L. Ribeiro, *J Sol-Gel Sci Techn*, 2009, **50**, 158-163.
13. M. A. P. Silva, D. F. Franco, A. R. Brandao, H. Barud, F. A. Dias, S. J. L. Ribeiro, Y. Messaddeq and L. F. C. de Oliveira, *Mater Chem Phys*, 2010, **124**, 547-551.
14. N. C. Masson, E. F. deSouza and F. Galembeck, *Colloid Surface A*, 1997, **121**, 247-255.
15. A. Momeni and M. J. Filiaggi, *J Rheol*, 2016, **60**, 25-34.
16. A. Momeni and M. J. Filiaggi, *Langmuir*, 2014, **30**, 5256-5266.
17. T. Umegaki and T. Kanazawa, *B Chem Soc Jpn*, 1975, **48**, 1452-1454.
18. V. A. Sinyaev, E. S. Shustikova, L. V. Levchenko and A. A. Sedunov, *Inorg Mater+*, 2001, **37**, 619-622.
19. F. A. Dias, L. D. Carlos, Y. Messadeq and S. J. L. Ribeiro, *Langmuir*, 2005, **21**, 1776-1783.
20. G. Willot, F. Gomez, P. Vast, W. Andries, M. Martines, Y. Messaddeq and M. Poulain, *Cr Chim*, 2002, **5**, 899-906.
21. E. F. deSouza, C. C. Bezerra and F. Galembeck, *Polymer*, 1997, **38**, 6285-6293.
22. R. Pfanstiel and R. K. Iler, *J Am Chem Soc*, 1956, **78**, 5510-5511.
23. A. Iost, R. Bigot, F. Barbieux and P. Vast, *J Mater Sci*, 1999, **34**, 3991-3996.
24. D. Priftis and M. Tirrell, *Soft Matter*, 2012, **8**, 9396-9405.
25. S. L. Perry, Y. Li, D. Priftis, L. Leon and M. Tirrell, *Polymers-Basel*, 2014, **6**, 1756-1772.
26. Q. F. Wang and J. B. Schlenoff, *Macromolecules*, 2014, **47**, 3108-3116.
27. W. C. Blocher and S. L. Perry, *Wires Nanomed Nanobi*, 2017, **9**.
28. A. Seweryn, T. Wasilewski and T. Bujak, *Ind Eng Chem Res*, 2016, **55**, 1134-1141.
29. E. Spruijt, A. H. Westphal, J. W. Borst, M. A. C. Stuart and J. van der Gucht, *Macromolecules*, 2010, **43**, 6476-6484.
30. J. P. Jones, M. Sima, R. G. O'Hara and R. J. Stewart, *Adv Healthc Mater*, 2016, **5**, 795-801.
31. J. M. Sanchezruiz and M. Martinezcarrion, *Biochemistry-Us*, 1988, **27**, 3338-3342.
32. N. N. Ashton and R. J. Stewart, *Soft Matter*, 2015, **11**, 1667-1676.
33. W. J. Wang, N. A. Anderson, A. Travesset and D. Vaknin, *J Phys Chem B*, 2012, **116**, 7213-7220.
34. E. E. Kooijman, K. M. Carter, E. G. van Laar, V. Chupin, K. N. J. Burger and B. de Kruijff, *Biochemistry-Us*, 2005, **44**, 17007-17015.
35. C. W. Bock, A. Kaufman and J. P. Glusker, *Inorg Chem*, 1994, **33**, 419-427.
36. G. D. Markham, J. P. Glusker and C. W. Bock, *J Phys Chem B*, 2002, **106**, 5118-5134.
37. D. Rutkowska-Zbik, M. Witko and L. Fiedor, *J Mol Model*, 2013, **19**, 4661-4667.
38. T. Dudev, J. A. Cowan and C. Lim, *J Am Chem Soc*, 1999, **121**, 7665-7673.
39. O. Allner, L. Nilsson and A. Villa, *J Chem Theory Comput*, 2012, **8**, 1493-1502.
40. A. K. Katz, J. P. Glusker, S. A. Beebe and C. W. Bock, *J Am Chem Soc*, 1996, **118**, 5752-5763.
41. M. E. Maguire and J. A. Cowan, *Biometals*, 2002, **15**, 203-210.
42. O. Carugo, K. Djinovic and M. Rizzi, *J Chem Soc Dalton*, 1993, **14**, 2127-2135.
43. H. Diebler, Eigen, M., Ilgenfritz, G., Maass, G., Winkler, R., *Pure and Applied Chemistry*, 1969, **20**, 14.
44. R. J. Stewart and C. S. Wang, *Biomacromolecules*, 2010, **11**, 969-974.
45. N. N. Ashton, D. R. Roe, R. B. Weiss, T. E. Cheatham and R. J. Stewart, *Biomacromolecules*, 2013, **14**, 3668-3681.
46. J. B. Addison, N. N. Ashton, W. S. Weber, R. J. Stewart, G. P. Holland and J. L. Yarger, *Biomacromolecules*, 2013, **14**, 1140-1148.
47. N. N. Ashton, H. Z. Pan and R. J. Stewart, *Open Biol*, 2016, **6**.
48. E. Spruijt, M. A. C. Stuart and J. van der Gucht, *Macromolecules*, 2013, **46**, 1633-1641.
49. R. G. Pearson, *J Am Chem Soc*, 1963, **85**, 3533-&.
50. P. C. Anthony, A. Y. L. Sim, V. B. Chu, S. Doniach, S. M. Block and D. Herschlag, *J Am Chem Soc*, 2012, **134**, 4607-4614.
51. J. C. Bowman, T. K. Lenz, N. V. Hud and L. D. Williams, *Curr Opin Struc Biol*, 2012, **22**, 262-272.
52. C. M. Frey and J. E. Stuehr, *J Am Chem Soc*, 1972, **94**, 8898-8904.
53. D. J. Klein, P. B. Moore and T. A. Steitz, *RNA*, 2004, **10**, 1366-1379.
54. J. R. Pawlik, *J Mar Biol Assoc Uk*, 1988, **68**, 101-124.
55. P. H. Yancey, M. E. Clark, S. C. Hand, R. D. Bowlus and G. N. Somero, *Science*, 1982, **217**, 1214-1222.